







Implementing Large Quantum Boltzmann Machines as Generative AI Models for Dataset Balancing

Salvatore Sinno ^{*†}, Markus Bertl ^{*†}, Arati Sahoo ^{*}, Bhavika Bhalgamiya ^{*},
Thomas Groß [†] and Nicholas Chancellor [†]

^{*}NextGen Computing Research Group, Unisys, Blue Bell, Pennsylvania, USA

Email: {salvatore.sinno, markus.bertl, arati.sahoo, bhavika.bhalgamiya}@unisys.com

[†]School of Computing, Newcastle University, Newcastle upon Tyne, United Kingdom

[‡]Department of Information Systems and Operations Management, Vienna University of Economics and Business, Austria

Abstract—This study explores the implementation of large Quantum Restricted Boltzmann Machines (QRBM), a key advancement in Quantum Machine Learning (QML), as generative models on D-Wave’s Pegasus quantum hardware to address dataset imbalance in Intrusion Detection Systems (IDS). By leveraging Pegasus’s enhanced connectivity and computational capabilities, a QRBM with 120 visible and 120 hidden units was successfully embedded, surpassing the limitations of default embedding tools. The QRBM synthesized over 1.6 million attack samples, achieving a balanced dataset of over 4.2 million records. Comparative evaluations with traditional balancing methods, such as SMOTE and RandomOversampler, revealed that QRBM produced higher-quality synthetic samples, significantly improving detection rates, precision, recall, and F₁ score across diverse classifiers. The study underscores the scalability and efficiency of QRBM, completing balancing tasks in milliseconds. These findings highlight the transformative potential of QML and QRBM as next-generation tools in data preprocessing, offering robust solutions for complex computational challenges in modern information systems.

Index Terms—Quantum Computing, Quantum Machine Learning (QML), Quantum Restricted Boltzmann Machines (QRBM), Restricted Boltzmann Machines (RBM), Dataset Balancing, Unbalanced Data, Generative Models, Intrusion Detection Systems.

I. INTRODUCTION

Balanced datasets have long been recognized as essential for effective machine learning (ML), enabling models to generalize and produce robust predictions. In the context of intrusion detection systems (IDS), the importance of balanced datasets becomes even more pronounced. IDS are critical for securing networks by identifying malicious activities amidst normal traffic. However, real-world datasets used for training IDS have often suffered from severe class imbalance, where the volume of normal traffic significantly outweighed that of intrusion attempts. This imbalance has limited the effectiveness of ML models, resulting in biased predictions favouring the majority class, reduced detection rates for rare but critical intrusions, and increased false positive rates.

The challenges posed by class imbalance were multifaceted. ML models trained on imbalanced datasets tended to optimize for the majority class, neglecting the minority class. Traditional balancing methods, such as oversampling and

undersampling or Synthetic Minority Oversampling Technique (SMOTE) [7], have significant drawbacks. Oversampling introduced redundancy and increased the risk of overfitting; undersampling often discarded valuable information from the majority class. SMOTE can not handle class boundaries effectively and has high-dimensional or sequential data challenges. These limitations underscored the need for novel approaches to address class imbalance in IDS datasets.

This study leveraged the potential of quantum computing to address these challenges, focusing specifically on quantum-restricted Boltzmann Machines (QRBM). QRBM, as generative models, can learn the statistical properties of datasets and synthesise realistic data samples. By utilising principles of quantum mechanics, QRBM could efficiently explore high-dimensional data spaces, making them particularly suited for generating synthetic data to balance imbalanced datasets. Unlike classical methods, QRBM exploited quantum superposition and entanglement to represent complex probability distributions more effectively, offering significant advantages in addressing class imbalance.

The results and contributions of the study are summarized as follows:

- **Largest QRBM Implementation:** Successfully implemented a large QRBM (120 visible and 120 hidden units) on D-Wave’s Pegasus architecture, overcoming the limitations of D-Wave’s default embedding tools. This implementation highlights the potential of QRBM to act as powerful generative models for balancing even the most complex datasets.
- **Generative Modeling for IDS:** Demonstrated the efficacy of QRBM in generating high-quality synthetic data, achieving superior precision, recall, and F₁ scores compared to traditional methods.
- **Improved IDS Performance:** Evaluated the impact of QRBM-generated datasets on IDS performance metrics. Results showed significant improvements in detection rates and reductions in false positives, demonstrating QRBM’s ability to enhance IDS reliability and robustness.

II. RELATED WORK

Class imbalance is a persistent challenge in ML, particularly in fields like IDS, where the normal traffic volume far exceeds intrusion events. Several classical methods have been proposed to address this imbalance, including SMOTE and Random Oversampling. SMOTE generates synthetic samples by interpolating between existing minority class samples, while Random Oversampling duplicates minority class samples to achieve balance [7], [12]. Although these methods improve dataset balance, they often lead to issues such as overfitting and redundancy, limiting their effectiveness in real-world scenarios [10] [19].

Previous studies, such as those by Gopalan et al. [11] and Abdulrahman et al. [1], emphasize balancing techniques for IDS datasets, highlighting the challenges of achieving fair evaluation metrics. Abdulrahman et al. [1] investigate balancing the CICIDS2017 dataset using classical techniques, which, while effective to some extent, often fail to capture nuanced feature interactions within the data. Liu et al. [18] propose using Generative Adversarial Networks (GANs) for data balancing, showcasing their potential in generating robust datasets for IDS tasks.

QRBM have emerged as a promising alternative to classical methods for handling imbalanced datasets. QRBM, an extension of classical Restricted Boltzmann Machines (RBMs), leverage the principles of quantum computing to model complex probability distributions and generate synthetic data. Unlike classical RBMs, QRBM utilize quantum annealing to efficiently sample from high-dimensional energy landscapes, making them particularly well-suited for generative tasks [3], [15]. Prior research has demonstrated the potential of QRBM in various machine-learning applications, including anomaly detection and classification tasks [3], [9].

Implementing QRBM on quantum hardware poses unique challenges, particularly concerning embedding large models on physical quantum processors. D-Wave's Chimera topology, an early quantum annealing architecture, provided limited qubit connectivity, which constrained the scalability of QRBM implementations [22]. The introduction of D-Wave's Pegasus topology addressed these limitations by offering enhanced qubit connectivity and increased computational capacity [16]. Recent studies have explored methods for minor embedding of problems on Pegasus, showcasing significant improvements in performance and scalability [8], [20].

The proposed algorithm demonstrates remarkable flexibility and efficiency in embedding RBMs on D-Wave's Pegasus architecture. It enables the minor embedding up to a 172x120 RBM by optimizing chain lengths to remain short while maximizing the utilization of qubits for visible and hidden nodes.

This algorithm outperforms D-Wave's default embedding tool. The ability to efficiently embed larger RBMs underscores the algorithm's potential to enhance quantum annealing applications, particularly in generative modelling and data balancing tasks.

III. RESTRICTED BOLTZMANN MACHINES

RBMs are stochastic neural networks that model the joint probability distribution of visible and hidden variables. They are energy-based models that learn to represent data by minimizing an energy function. RBMs consist of two layers: a visible layer \mathbf{v} representing observed data and a hidden layer \mathbf{h} that captures latent features. There are no intra-layer connections, simplifying the computation and making the model tractable [15].

The energy of a configuration (\mathbf{v}, \mathbf{h}) of the visible and hidden units in an RBM is defined as:

$$E(\mathbf{v}, \mathbf{h}) = - \sum_{i \in \text{visible}} b_i v_i - \sum_{j \in \text{hidden}} c_j h_j - \sum_{i,j} v_i W_{ij} h_j, \quad (1)$$

where b_i and c_j are biases for the visible and hidden units, respectively, and W_{ij} represents the weights of the connection between visible unit i and hidden unit j . This energy function determines the likelihood of a given configuration; lower energy corresponds to higher probability.

The joint probability of a visible vector \mathbf{v} and a hidden vector \mathbf{h} is expressed using the Boltzmann distribution:

$$P(\mathbf{v}, \mathbf{h}) = \frac{\exp(-E(\mathbf{v}, \mathbf{h}))}{Z}, \quad (2)$$

where Z is the partition function defined as:

$$Z = \sum_{\mathbf{v}, \mathbf{h}} \exp(-E(\mathbf{v}, \mathbf{h})). \quad (3)$$

The partition function normalizes the probability distribution, ensuring that $P(\mathbf{v}, \mathbf{h})$ is valid.

A. Conditional Independence and Sampling

One of the key features of RBMs is that the visible and hidden units are conditionally independent of each other. This allows efficient sampling from the distribution:

$$P(h_j = 1 | \mathbf{v}) = \sigma \left(c_j + \sum_i W_{ij} v_i \right), \quad (4)$$

$$P(v_i = 1 | \mathbf{h}) = \sigma \left(b_i + \sum_j W_{ij} h_j \right), \quad (5)$$

where $\sigma(x)$ is the sigmoid function $\sigma(x) = 1/(1 + e^{-x})$. This property enables Gibbs sampling for training and inference.

RBMs are trained by maximizing the likelihood of the observed data \mathbf{v} . Direct computation of the log-likelihood gradient is intractable due to the partition function Z . To overcome this, Contrastive Divergence (CD) is used as an approximation [13]. The update rule for the weights is given by:

$$\Delta W_{ij} = \langle v_i h_j \rangle_{\text{data}} - \langle v_i h_j \rangle_{\text{model}}, \quad (6)$$

where $\langle \cdot \rangle_{\text{data}}$ represents expectations under the data distribution, and $\langle \cdot \rangle_{\text{model}}$ represents expectations under the model distribution.

B. RBMs as Generative Models

RBMs can be used as generative models as they learn and replicate a dataset's statistical properties. Once trained, an RBM can generate new data samples by alternately sampling from the visible and hidden layers in a process known as Gibbs sampling [6]. This iterative sampling process alternates between activating the hidden units based on the visible units and vice versa, gradually producing new visible configurations that align with the learned data distribution.

This generative capability makes RBMs a powerful tool for several applications. One of their primary uses is in dataset augmentation, where new data samples are synthesized to address challenges like limited data availability or class imbalance. For example, in highly imbalanced datasets, an RBM can generate synthetic samples for under-represented classes, effectively increasing their prevalence and improving the performance of downstream supervised learning models [14]. Unlike oversampling techniques that merely duplicate existing data points, RBMs generate entirely new samples that preserve the statistical diversity of the dataset, reducing the risk of overfitting.

C. Quantum Extensions

In quantum computing, the concept of generative modelling with RBMs has been extended to QRBMs. QRBMs enhance the generative capabilities of RBMs by leveraging quantum effects such as superposition and entanglement, enabling them to sample from high-dimensional and complex probability distributions efficiently. These properties make QRBMs particularly suitable for generating synthetic data in large-scale, complex applications such as anomaly detection and advanced generative tasks [3].

A key aspect of implementing QRBMs lies in mapping the RBM energy function to the Ising model [5], a well-studied model in quantum mechanics and statistical physics. An energy function defines the Ising model:

$$H = - \sum_i h_i s_i - \sum_{i < j} J_{ij} s_i s_j, \quad (7)$$

where $s_i \in \{-1, +1\}$ are spin variables, h_i are local biases, and J_{ij} are coupling coefficients between spins. The Ising model is the basis for quantum annealers, such as those developed by D-Wave Systems. The RBM energy function (Equation 1) can be reformulated into an equivalent Ising Hamiltonian by encoding the visible and hidden units as spin variables, their biases as local fields, and their weights as couplings between spins. This mapping enables the direct implementation of RBM-like models on quantum hardware [2].

Quantum annealing trains QRBMs by finding low-energy configurations of the Ising Hamiltonian, which correspond to the most probable configurations in the RBM's probability distribution. This is particularly advantageous in high-dimensional and multimodal distributions, where classical methods often struggle due to local minima and high computational costs. By leveraging tunnelling, quantum annealers

can escape local minima and explore the solution space more effectively. In this way, QRBMs are particularly suitable for generating synthetic data in applications like class imbalance correction, where they outperform classical oversampling techniques by better preserving the statistical properties of minority classes [4]. Advanced quantum architectures, such as D-Wave's Pegasus topology, have enabled QRBMs to scale to larger problem sizes. The Pegasus topology provides improved qubit connectivity, allowing for more efficient embeddings of the Ising Hamiltonian corresponding to large RBMs. This advancement has opened new possibilities for tackling real-world problems, such as optimizing supply chains, enhancing cybersecurity systems, and advancing generative modelling for machine learning applications.

IV. METHODOLOGY

Fig. 1 illustrates the process for addressing the challenge of dataset imbalance using a QRBM. The workflow begins with the initial dataset, divided into two key components: training and testing data.

The training data is split into attack datasets, and then the attack dataset undergoes a binarization process, converting the data into a binary format suitable for analysis by the QRBM. The QRBM is trained on the binarized attack data to generate synthetic data, which mirrors the underlying distribution and characteristics of the original attack data.

Combining synthetic data with the original training data produces a balanced dataset, ensuring that classes or data categories are equally represented. This newly balanced dataset is then used to train classifiers to identify patterns and make predictions based on the input data.

Once the classifiers are trained, their performance is evaluated using the testing data. The predictions generated by the classifiers are compared against the actual outcomes in the testing data to assess the model's accuracy, reliability, and overall effectiveness. The final step involves a comprehensive analysis of the prediction results, which provides valuable insights into the success of the balancing process and the performance of the classifiers.

A. Dataset Preparation

The study utilized the CICIDS2017 dataset, a comprehensive benchmark dataset developed by the Canadian Institute for Cybersecurity. CICIDS2017 is widely recognized for its relevance in evaluating IDS due to its diversity and realistic simulation of modern network traffic. The dataset captures a balanced representation of regular activity and various attack scenarios, providing a robust foundation for developing and testing advanced machine learning and quantum-based models [21].

CICIDS2017 was created to address the shortcomings of earlier datasets, such as outdated attack types, lack of feature diversity, and unrealistic traffic generation. It includes over 3 million network flow records collected over 5 days, encompassing a mix of benign and malicious traffic. The malicious activities are categorized into six distinct attack types. The

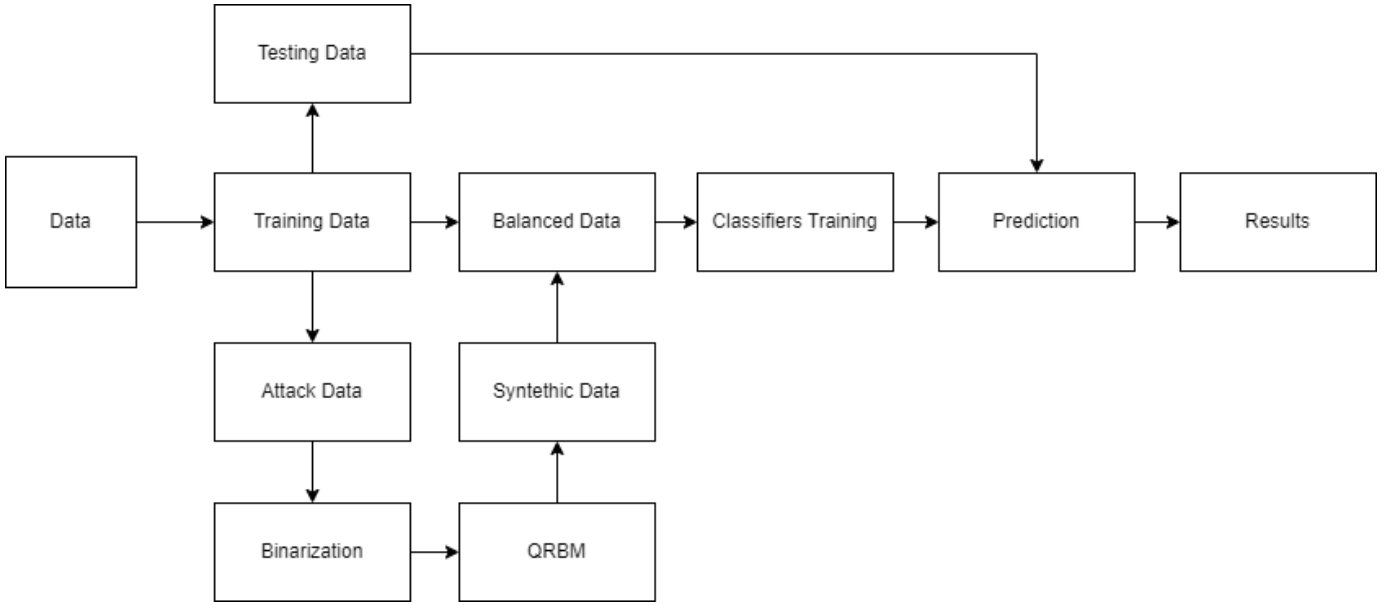


Fig. 1. Flow chart for balancing a dataset using QRBMs.

dataset is structured with over 83 features extracted using network flow analysis tools [17]. The feature richness makes CICIDS2017 an ideal dataset for testing anomaly detection systems and advanced generative modelling techniques.

Despite its comprehensiveness, the CICIDS2017 exhibits significant imbalance, with benign traffic far outnumbering malicious activity. Attack categories are severely under-represented, necessitating synthetic data augmentation using QRBMs to balance the dataset.

TABLE I
OVERALL CHARACTERISTICS OF CICIDS2017 DATASET

Dataset Type	Multiclass
Year of Release	2017
Total Number of distinct instances	2,830,540
Number of features	83
Number of distinct classes	15

Table I provides the overall characteristics of the CICIDS2017 dataset, while Table II provides an overview of the class distribution of the dataset.

B. QRBMs Implementation on Pegasus Topology

The Pegasus topology provides advanced qubit connectivity, with each qubit connecting to up to 15 others, making it ideal for embedding larger and more complex QRBMs¹. This study developed an algorithm to implement large QRBMs (up to 172x120) on the Pegasus topology.

Our embedding algorithm (Algorithm 1) maps the visible and hidden units of the QRBMs to physical qubits. It allows

TABLE II
CLASS INSTANCES CICIDS2017 DATASET

Class Labels	Number of instances
BENIGN	2,359,087
DoS Hulk	231,072
PortScan	158,930
DDoS	41,835
FTP-Patator	7,938
SSH-Patator	5,897
DoS slowloris	5,897
DoS Slowhttptest	5,499
Bot	1,966
Web Attack - Brute Force	1,507
Web Attack - XSS	652
Infiltration	36
Web Attack - Sql Injection	21
Heartbleed	11

for shorter qubit chains, reducing the risk of chain breakage and improving the accuracy of the annealing process.

Although the Pegasus architecture supports increased connectivity and enables larger embeddings, managing qubit allocation for increasingly complex QRBMs remains challenging. Preserving the bipartite structure of the QRBMs and maintaining the integrity of interactions between visible and hidden units during physical embedding is critical. Our algorithm outperforms D-Wave's default embedding tool (`minorminer.find_embedding`) as shown in Table III. In contrast, our algorithm efficiently identifies multiple QRBMs configurations (ranging from 4x4 to 172x120) in milliseconds, eliminating the need for manual adjustments when the QRBMs structure changes. Once the embedding is generated, the graph

¹https://docs.dwavesys.com/docs/latest/c_gs_4.html

is passed to the annealer using the J and h matrices, ensuring seamless integration into the quantum computation process.

TABLE III
COMPARISON OF EMBEDDING ALGORITHMS FOR DIFFERENT CONFIGURATIONS

Algorithm	Metric	60x60	120x120
Our Algorithm	Avg. Time (s)	0.012	0.014
	Std. Deviation (s)	0.0012	0.0011
	Avg. Chains with length > 6	0	0
Minorminer	Avg. Time (s)	214.94	960.02
	Std. Deviation (s)	108.75	170.35
	Avg. Chains with length > 6	2	15

Our algorithm begins by determining how the visible and hidden nodes are arranged on the processor. The number of visible and hidden nodes is divided into vertical and horizontal segments based on periodicity parameters, which dictate the spacing and structure of the node embeddings. Starting indices are defined for visible and hidden nodes based on the physical layout of the Quantum Processing Unit (QPU), guiding the placement of nodes within their respective layers. The mapping process involves iterating through these segments and assigning physical qubits to logical nodes. At the same time, couplings within each layer are identified and repeated across the QPU, ensuring that the intra-layer relationships are fully captured.

Once the nodes within each layer are mapped, the algorithm establishes inter-layer connections between visible and hidden nodes. This step pairs nodes from the two layers based on their logical indices and periodicity. These connections are stored as part of the coupling data and are later used to populate the coupling matrix. The algorithm's output includes the coupling matrix, visible and hidden node lists, and detailed intra-layer and inter-layer coupling records.

C. Experimental Setup

The experiments were conducted using a hybrid setup. A Dell R705X server with 128 logical cores and 503 GiB of RAM was utilized to perform classical machine learning tasks. The server ran Ubuntu 22.04 and Python 3.10.9 with Scikit-learn 1.5.2, and minorminer 0.2.16. SMOTE and RandomOverSampler were implemented to address the class imbalance. The QRBm balanced the datasets by generating 1,000 samples of attack class data in each anneal, with D-Wave's default annealing time of $20\mu s$ and $124\mu s$ for readout.

The evaluation metrics adopted were precision, recall, and F_1 scores, calculated across several classifiers: Support Vector Machines (SVM), Logistic Regression, Naïve Bayes, Decision Trees, Gradient Boosting, K-Nearest Neighbors (KNN), and Random Forest.

1) *Data Preprocessing*: The preprocessing involved converting the dataset into a binary format compatible with the QRBm. Steps included normalization, encoding, and feature transformation to enhance the data's quality and compatibility. Handling missing values was crucial in preprocessing the dataset, as unaddressed gaps could lead to biased or inaccurate models. Missing values in the dataset were addressed

using mean and median imputation techniques, with invalid or incorrect entries removed to improve data integrity. In total, 1,305 NaN values and 1,310 infinite values were identified and eliminated from the dataset. A correlation analysis was conducted to identify features with strong associations to address redundancy. Highly correlated features (absolute correlation ≥ 0.9) and features with zero standard deviation were deemed redundant and removed. In total, 23 features with high correlations and eight with zero variance were removed, leaving 48 meaningful features. Duplicate records were identified and removed to prevent bias in the models. 307,078 duplicate entries were removed, leaving a final dataset of 2,524,847 records. This included 2,104,309 benign samples and 420,538 attack samples (Table IV).

Key features were extracted based on their significance in intrusion detection tasks and encoded into binary form using equation 8:

$$\text{Max}(\text{feature_value}) - \text{Min}(\text{feature_value}) \leq 2^N \quad (8)$$

where N is the number of bits required for encoding.

At the end of this process, we created a 120-bit vector, and we selected a QRBm with 120 visible and 120 hidden units.

D. Balancing the Dataset using the QRBm

The QRBm was trained using Algorithm 2, adapted from [9], and the resulting parameters (W, b, c) were utilized in the embedding process via Algorithm 1. Each quantum annealing step produced 1,000 samples in milliseconds, with the visible unit states forming individual entries in the synthetic dataset. Repeating this process 1,700 times resulted in 1,683,771 synthetic attack samples, creating a perfectly balanced dataset of 4,208,618 samples. With each annealing process lasting only $20\mu s$, we rapidly generated high-quality synthetic data.

TABLE IV
TRAIN/TEST SPLIT

	Total	Benign	Attack
Training	1,767,393	1,473,016	294,377
Test	757,454	631,293	126,161
Total	2,524,847	2,104,309	420,538

V. RESULTS

The results are tabulated and compared for four types of datasets: without balancing, balancing using SMOTE, RandomOverSampler, and QRBm.

Table V shows the time taken to balance the dataset using three different models: SMOTE, Random Over Sampler and QRBm. The SMOTE and Random Over Sampler methods took a relatively short time (0.75 and 0.23 seconds, respectively), and only 0.33 seconds for the QRBm.

Table VI shows the results of the evaluation metrics obtained when the dataset was trained without balancing the dataset.

Table VII shows the results of the evaluation metrics obtained when the dataset was trained and modelled after balancing it using SMOTE.

Table VIII shows the results of the evaluation metrics obtained

when the dataset was trained and modelled after balancing it using RandomOverSampler.

Table IX shows the results of the evaluation metrics obtained when the dataset was trained and modelled after balancing it using QRBM.

TABLE V
TIME TAKEN TO BALANCE THE DATASET

	SMOTE	RandomOverSampler	QRMB
Time(s)	0.75	0.23	0.33

TABLE VI
EVALUATION METRICS WITHOUT BALANCING

Model	Precision	Recall	F ₁ Score
SVM	24.67	25.81	24.84
Naïve Bayes	51.81	47.27	27.04
Logistic Regression	24.74	24.95	24.84
Gradient Boosting	54.74	54.46	54.24
KNN	48.7	46.94	47.75
Decision Tree	50.35	51.17	50.41
Random Forest	77.3	50.97	53.29

TABLE VII
EVALUATION METRICS AFTER BALANCING USING SMOTE

Model	Precision	Recall	F ₁ Score
SVM	74.8	63.63	57.69
Naïve Bayes	70.18	70.32	64.14
Logistic Regression	77.93	70.88	64.84
Gradient Boosting	85.79	85.42	85.31
KNN	85.53	85.67	85.6
Decision Tree	86.73	86.7	86.5
Random Forest	89.49	89.51	89.5

SVM shows a precision of 74.8%, recall of 63.63%, and an F₁ score of 57.69%, indicating a balanced performance with substantial improvements compared to the unbalanced scenario. Naïve Bayes also exhibits balanced metrics, with precision at 70.18%, recall at 70.32%, and an F₁ score of 64.14%. Logistic Regression shows slightly higher metrics, with precision at 77.93%, recall at 70.88%, and an F₁ score of 64.84%, demonstrating good model performance after balancing.

Gradient Boosting, KNN, and Random Forest stand out with significantly higher metrics. Gradient Boosting has precision, recall, and F₁ scores of approximately 85.4%, while KNN shows similar consistency across the metrics with scores around 85.6%. Random Forest leads with the highest precision at 89.49%, recall at 89.51%, and an F₁ score of 89.5%, indicating superior performance in the balanced dataset.

Decision Tree also shows strong performance with precision at 86.73%, recall at 86.7%, and an F₁ score of 86.5%, highlighting its effectiveness after SMOTE balancing.

Table VIII shows that SVM reached a precision of 74.86%, recall of 63.55%, and an F₁ score of 57.57%, indicating a balanced performance with substantial improvements compared to the unbalanced scenario. Naïve Bayes also displays balanced metrics, with precision at 67.24%, recall at 69.69%,

TABLE VIII
EVALUATION METRICS AFTER BALANCING USING
RANDOMOVERSAMPLER

Model	Precision	Recall	F ₁ Score
SVM	74.86	63.55	57.57
Naïve Bayes	67.24	69.69	63.05
Logistic Regression	78.2	70.74	64.63
Gradient Boosting	87.41	87.03	86.95
KNN	90.67	90.50	90.5
Decision Tree	96.08	95.98	95.99
Random Forest	96.05	95.95	95.96

and an F₁ score of 63.05%. Logistic Regression exhibits slightly higher metrics, with precision at 78.2%, recall at 70.74%, and an F₁ score of 64.63%, demonstrating good model performance after balancing.

Gradient Boosting, KNN, and Random Forest stand out with significantly higher metrics. Gradient Boosting shows precision, recall, and F₁ scores around 87.03% to 87.41%, while KNN demonstrates high consistency across the metrics with scores around 90.5%. Random Forest and Decision Tree lead with the highest metrics, where Decision Tree has a precision of 96.08%, recall of 95.98%, and an F₁ score of 95.99%, while Random Forest follows closely with a precision of 96.05%, recall of 95.95%, and an F₁ score of 95.96%, indicating superior performance in the balanced dataset.

TABLE IX
EVALUATION METRICS AFTER BALANCING USING QRBM

Model	Precision	Recall	F ₁ Score
SVM	75.19	63.67	57.67
Naïve Bayes	67.68	69.77	63.11
Logistic Regression	77.08	70.6	64.28
Gradient Boosting	87.94	87.54	87.46
KNN	91.15	90.93	90.91
Decision Tree	95.94	95.87	95.87
Random Forest	96.18	96.1	96.1

Table IX illustrates various models' evaluation metrics (Precision, Recall, F₁ Score) after balancing using QRBM. The Random Forest achieves the highest precision at 96.18%, and the Decision Tree follows closely with a precision of 95.94%. KNN also performs well with a precision of 91.15%. Other models like Gradient Boosting, Logistic Regression, Naïve Bayes, and SVM have progressively lower precision values. Tree-based methods like Random Forests and Decision Trees demonstrate the best overall performance across all metrics. KNN also performs well but with slightly lower values. While effective, Gradient Boosting, Logistic Regression, Naïve Bayes, and SVM do not achieve the same high precision, recall, and F₁ scores as the top-performing models.

VI. DISCUSSION

QRBM achieved superior performance compared to classical methods, such as SMOTE and RandomOverSampler, by generating high-quality synthetic samples that improved evaluation metrics like precision, recall, and F₁ scores across multiple ML models. Furthermore, QRBM demonstrated re-

markable time efficiency, completing the balancing process in just 0.33 seconds, as shown in Table V.

QRBM exhibits clear advantages over classical methods such as SMOTE and RandomOverSampler by efficiently generating high-quality synthetic data using quantum annealing to model complex interactions. Unlike statistical approaches, QRBM captures probabilistic dependencies across features, allowing for more nuanced sample generation. This capability is particularly critical in IDS applications, where the distribution of attack vectors is intricate and highly non-uniform, requiring sophisticated modelling techniques to ensure effective data balancing and robust detection.

The comparison of QRBM with deep learning-based generative models, such as GANs, further highlights their unique advantages. While GANs can learn from data distributions and generate high-quality synthetic samples, they face challenges like mode collapse and demand significant computational resources, particularly for large-scale datasets. In contrast, QRBM leverages quantum hardware to model energy landscapes directly, offering rapid sampling and scalability. Unlike GANs, QRBM circumvents extensive training and hyperparameter tuning, making them a more efficient choice in specific scenarios. However, QRBM has limitations, as quantum hardware restricts scalability due to limited qubit counts and noise. Additionally, hybrid quantum-classical workflows introduce complexities in preprocessing and postprocessing, requiring further advancements in hardware and algorithms to realize their full potential. Future research should include direct comparisons between QRBM and GANs, focusing on computational efficiency, sample diversity, and downstream IDS performance.

QPU sampling time (134.92 μs) and readout time (94 μs) illustrate QRBM's capability to generate synthetic samples rapidly. Unlike classical methods, QRBM maintains consistent runtimes across varying dataset sizes, making them well-suited for large-scale data preprocessing tasks.

QRBM faces challenges due to the limitations of current quantum hardware. Issues such as limited qubit connectivity, short coherence times, and error rates can impact their performance. Moreover, QRBM workflows' hybrid nature, combining quantum and classical computations, introduces additional data preprocessing and postprocessing complexity. The introduction of the Zephyr topology, with its enhanced qubit connectivity and density, has the potential to mitigate many of these hardware limitations, enabling the embedding of larger and more complex QRBM while reducing chain breaks and improving sampling quality. Additionally, Zephyr's improved scalability and efficiency could streamline hybrid quantum-classical workflows by simplifying preprocessing and embedding steps, further unlocking the potential of QRBM in real-world applications.

Future research should focus on overcoming these challenges through advancements in quantum hardware and optimization techniques, in particular, developing more efficient embedding strategies to scale QRBM implementations for even larger and more complex datasets, exploring alternative

quantum architectures and algorithms to optimize QRBM performance further and expanding the application of QRBM in domains like healthcare, finance, and other real-time anomaly detection fields.

VII. CONCLUSION

This study has demonstrated the potential of quantum-restricted Boltzmann Machines (QRBM) as a powerful tool for addressing dataset imbalances e.g., in intrusion detection systems (IDS). By leveraging the advanced capabilities of the Pegasus architecture, we successfully implemented one of the largest QRBM embedded on D-Wave's quantum processor to date, with 120 visible and 120 hidden units. Notably, this scale of QRBM exceeds the capabilities of D-Wave's default embedding tools, highlighting the significance of this achievement in generative modelling and quantum computing.

QRBM generated high-quality synthetic data, significantly improving IDS performance across multiple metrics, including precision, recall, and F_1 scores. Compared to classical techniques such as SMOTE and RandomOverSampler, QRBM provided superior results while maintaining remarkable computational efficiency. QRBM's generative modelling capability, supported by the enhanced connectivity and flexibility of the Pegasus topology, enabled efficient sampling from complex energy landscapes, overcoming the limitations of classical approaches like Gibbs sampling.

We therefore contribute by demonstrate the practical feasibility of large-scale QRBM implementations, pushing the boundaries of what can be achieved on existing quantum hardware.

REFERENCES

- [1] Amer Abdulmajeed Abdulrahman and Mahmood Khalel Ibrahim. Toward constructing a balanced intrusion detection dataset based on cicids2017. *Samarra Journal of Pure and Applied Science*, 2(3):132–142, 2020.
- [2] Shin Adachi and Maxwell P Henderson. Application of quantum annealing to training of deep neural networks. *arXiv preprint arXiv:1510.06356*, 2015.
- [3] Mohammad H Amin, Evgeny Andriyash, Jason Rolfe, Bohdan Kulchyskyi, and Roger Melko. Quantum boltzmann machine. *Physical Review X*, 8(2):021050, 2018.
- [4] Marcello Benedetti, John Realpe-Gomez, Rupak Biswas, and Alejandro Perdomo-Ortiz. Estimation of effective temperatures in quantum annealers for sampling applications: A case study with restricted boltzmann machines. *Physical Review A*, 94(2):022308, 2016.
- [5] Zhengbing Bian, Fabian Chudak, William G Macready, and Geordie Rose. The ising model: teaching an old problem new tricks. *D-wave systems*, 2:1–32, 2010.
- [6] George Casella and Edward I George. Explaining the gibbs sampler. *The American Statistician*, 46(3):167–174, 1992.
- [7] Nitesh V Chawla, Kevin W Bowyer, Lawrence O Hall, and W Philip Kegelmeyer. Smote: synthetic minority over-sampling technique. *Journal of artificial intelligence research*, 16:321–357, 2002.
- [8] Nike Dattani, Szilard Szalay, and Nicholas Chancellor. Pegasus: The second connectivity graph for large-scale quantum annealing hardware. *arXiv preprint arXiv:1901.07636*, 2019.
- [9] Akash Dixit, Rahul Sharma, and Priya Singh. Quantum-assisted training of restricted boltzmann machines. *Quantum Information Processing*, 22(5):135–150, 2023.
- [10] Vicente García, José Salvador Sánchez, and Ramón Alberto Mollineda. On the effectiveness of preprocessing methods when dealing with different levels of class imbalance. *Knowledge-Based Systems*, 25(1):13–21, 2012.

- [11] Subiksha Srinivasa Gopalan, Dharshini Ravikumar, Dino Linekar, Ali Raza, and Maheen Hasib. Balancing approaches towards ml for ids: a survey for the cse-cic ids dataset. In *2020 International Conference on Communications, Signal Processing, and their Applications (ICCSPA)*, pages 1–6. IEEE, 2021.
- [12] Haibo He and Edwardo A Garcia. Learning from imbalanced data. *IEEE Transactions on knowledge and data engineering*, 21(9):1263–1284, 2008.
- [13] Geoffrey E Hinton. Training products of experts by minimizing contrastive divergence. *Neural computation*, 14(8):1771–1800, 2002.
- [14] Geoffrey E Hinton. A practical guide to training restricted boltzmann machines. *Momentum*, 9:1–10, 2012.
- [15] Geoffrey E Hinton and Ruslan R Salakhutdinov. Reducing the dimensionality of data with neural networks. *Science*, 313(5786):504–507, 2006.
- [16] D-Wave Systems Inc. Pegasus topology, 2020.
- [17] Arash Habibi Lashkari, Gilberto Draper-Gil, Md Mamun, and Ali A Ghorbani. Characterization of tor traffic using time based features. *Proceedings of the 3rd International Conference on Information Systems Security and Privacy*, pages 253–262, 2017.
- [18] I-Hsien Liu, Cheng-En Hsieh, Wei-Min Lin, Jung-Shian Li, and Chu-Fen Li. Data-balancing algorithm based on generative adversarial network for robust network intrusion detection. *Journal of Robotics, Networking and Artificial Life*, 9(3):303–308, 2022.
- [19] Roweida Mohammed, Jumanah Rawashdeh, and Malak Abdullah. Machine learning with oversampling and undersampling techniques: overview study and experimental results. In *2020 11th international conference on information and communication systems (ICICS)*, pages 243–248. IEEE, 2020.
- [20] Elijah Pelofske. 4-clique network minor embedding for quantum annealers. *arXiv preprint arXiv:2301.08807*, 2023.
- [21] Iman Sharafaldin, Arash Habibi Lashkari, and Ali A Ghorbani. Toward generating a new intrusion detection dataset and intrusion traffic characterization. *ICISSp*, 1:108–116, 2018.
- [22] Davide Venturelli, Dominique J Marchand, and Gian-Luca Rojo. Quantum optimization of fully connected spin glasses. *Physical Review X*, 5(3):031040, 2015.

APPENDIX

A. Algorithms

Algorithm 1 Embedding a QRBm on Pegasus

```

1: Input:  $n_{\text{visible}}, n_{\text{hidden}}, \text{periodicity}_v,$ 
    $\text{periodicity}_h, n_{\text{periodicity}}$ 
2: Output: Logical-physical mappings for visible and
   hidden nodes, coupling matrix  $J$ 
3:  $H_V \leftarrow n_{\text{visible}}/n_{\text{periodicity}}$ 
4:  $H_H \leftarrow n_{\text{hidden}}/n_{\text{periodicity}}$ 
5: Initialize  $J_{\text{coupling}}, \text{visible\_nodes}, \text{hidden\_nodes},$ 
   and  $J_{\text{connections}}$  as empty lists
6:  $\text{startv} \leftarrow \text{periodicity}_v$ 
7: for  $z \leftarrow 0$  to  $H_V - 1$  do
8:   for  $x \leftarrow 0$  to  $n_{\text{periodicity}} - 1$  do
9:      $n \leftarrow \text{startv} + (n_{\text{periodicity}} \cdot x) + (z \cdot \text{periodicity}_v)$ 
10:    Append  $n$  to  $\text{visible\_nodes}$ 
11:    for  $j \leftarrow 0$  to  $H_H - 2$  do
12:      Append  $(n + j, n + j + 1)$  to  $J_{\text{coupling}}$ 
13:    end for
14:  end for
15: end for
16:  $\text{starto} \leftarrow \text{periodicity}_h$ 
17: for  $z \leftarrow 0$  to  $H_H - 1$  do
18:   for  $x \leftarrow 0$  to  $n_{\text{periodicity}} - 1$  do

```

```

19:    $p \leftarrow \text{starto} + (n_{\text{periodicity}} \cdot x) + (z \cdot \text{periodicity}_h)$ 
20:   Append  $p$  to  $\text{hidden\_nodes}$ 
21:   for  $j \leftarrow 0$  to  $H_V - 2$  do
22:     Append  $(p + j, p + j + 1)$  to  $J_{\text{coupling}}$ 
23:   end for
24: end for
25: end for
26: for  $x \leftarrow 0$  to  $H_H - 1$  do
27:   for  $y \leftarrow 0$  to  $H_V - 1$  do
28:     for  $t \leftarrow 0$  to  $n_{\text{periodicity}} - 1$  do
29:        $n \leftarrow \text{startv} + (n_{\text{periodicity}} \cdot t) + y \cdot \text{periodicity}_v + x$ 
30:       for  $k \leftarrow 0$  to  $n_{\text{periodicity}} - 1$  do
31:          $p \leftarrow \text{starto} + (n_{\text{periodicity}} \cdot k) + x \cdot \text{periodicity}_h + y$ 
32:         Append  $(n, p)$  to  $J_{\text{connections}}$ 
33:       end for
34:     end for
35:   end for
36: end for
37:  $J \leftarrow 0$ 
38: for Each  $(a, b)$  in  $J_{\text{coupling}}$  do
39:    $J[a, b] \leftarrow -1$ 
40: end for
41: return  $J, \text{visible\_nodes}, \text{hidden\_nodes}, J_{\text{coupling}},$ 
    $J_{\text{connections}}$ 

```

Algorithm 2 Training of a QRBm using quantum annealing (based on [9])

```

1:  $\epsilon \leftarrow \text{learning rate}$ 
2:  $b, c, W \leftarrow \text{random number}$ 
3: while not converged do
4:   Sample a mini-batch of  $m$  examples  $\{x^{(1)}, \dots, x^{(m)}\}$ 
   from the training set
5:    $V \leftarrow \{x^{(1)}, \dots, x^{(m)}\}$ 
6:    $H \leftarrow \sigma(c + VW)$ 
7:    $\{h, J\} \leftarrow \{b, c, W\}$ 
8:    $(V', H') \leftarrow \text{quantum annealing}(h, J)$ 
9:    $W \leftarrow W + \epsilon \left( \frac{V^T H}{m} - \frac{V'^T H'}{m_1} \right)$ 
10:   $b \leftarrow b + \epsilon \left( \frac{\text{sum}(V)}{m} - \frac{\text{sum}(V')}{m_1} \right)$ 
11:   $c \leftarrow c + \epsilon \left( \frac{\text{sum}(H)}{m} - \frac{\text{sum}(H')}{m_1} \right)$ 
12: end while

```
